



Predictions of the electrical conductivity and charging of the cloud particles in Jupiter's atmosphere

R. C. Whitten,¹ W. J. Borucki,² K. O'Brien,³ and S. N. Tripathi⁴

Received 27 July 2007; revised 16 November 2007; accepted 27 December 2007; published 1 April 2008.

[1] The electrical conductivity and electrical charge on cloud particles (composed of ammonia, ammonium hydrosulfide, and water) in the atmosphere of Jupiter are computed for pressures between 5.5 and 0.1 bars. The source of ionization is galactic cosmic rays (GCR). The distribution of charge among the various reservoirs is a function of altitude and the total area of the aerosol particles. For pressures below 4 bars, the electrons are scavenged efficiently by the cloud particles, decreasing the electron-ion recombination rate and resulting in increased positive ion abundance over that in the absence of the particles. For the upper regions of each cloud layer, the area of the aerosols and the large diffusion rate of the electrons cause most aerosol particles to be negatively charged. Near the bases of the cloud layers, the larger total area of the aerosols causes most of the charge, positive and negative, to reside on particles. Where clouds are present, the reduction of the electron conductivity ranges from a factor of 30 at 0.1 bar to 10^4 at 4 bars. At pressures near 1 bar and 4 bars, the positive ion conductivity increases by a factor of 10 over that expected for the clear atmosphere. A parametric study of negative ions shows that they are likely to be insignificant. For altitudes below the 0.3-bar level the predicted positive and negative conductivities are well below the detection limit of the relaxation and mutual impedance instruments such as those employed on the Huygens entry probe.

Citation: Whitten, R. C., W. J. Borucki, K. O'Brien, and S. N. Tripathi (2008), Predictions of the electrical conductivity and charging of the cloud particles in Jupiter's atmosphere, *J. Geophys. Res.*, 113, E04001, doi:10.1029/2007JE002975.

1. Introduction

[2] Now that the survey phase of the outer planets is nearly complete, future missions to Jupiter and the outer planets [Atreya and Wong, 2005; Space Studies Board and National Research Council, 2003; Wilson, 2004] will ask more detailed questions about the processes occurring in those atmospheres. In particular the increased use of entry probes to determine the in situ composition, photochemistry, electron and ion conductivity, abundances of ion and minor constituents, and aerosol properties and distributions is expected. Ionization by solar UV is important at the highest altitudes, but at the altitudes characteristic of the cloud layers' high-energy galactic cosmic ray particles (GCR) become the dominant source of ionization. For the case of atmospheres without electrophilic species, the loss of electrons generated by the GCR is greatly affected by the aerosols. In turn, their growth rates are affected by the charges they pick up because of the repulsion of like charge particles and the attraction of unlike charged particles

[Fuchs, 1961; Friedlander, 1977; Twomey, 1977]. Here we focus our attention on charged particle abundances and electron and positive ion conductivities since these properties are the most likely candidates for measurements (e.g., by a relaxation probe) in a future mission.

[3] In the present paper we employ the model of the Jovian atmosphere of Seiff *et al.* [1998] to compute updated ionization rates in the atmosphere at a range of latitudes due to GCR [O'Brien, 1971, 1975a, 1975b, 2005] and the altitude/pressure range in which clouds are present. The necessary conversion of magnetic latitudes to system III latitudes and longitudes was done by means of standard spherical trigonometry within the GCR ionization program. The density distributions of cloud particle concentrations are based on recent theoretical results of Atreya and Wong [2005], while radii are based on various measurements summarized by West *et al.* [2004]. Electron mobilities in hydrogen and helium were taken from the work of Ramanan and Freeman [1990, 1991], while ion mobilities were obtained from the work of Meyerott *et al.* [1980].

[4] Photoionization at the atmospheric depths at which the clouds occur is neglected because of absorption of solar ultraviolet ionizing radiation by methane and minor hydrocarbon constituents. Moreover, the intensity of the solar radiation is reduced by a factor of 25 below the value at the Earth's orbit, thus enhancing the relative importance of the GCR. We also omit photoemission of electrons by the cloud particles due to the impact of solar ultraviolet photons. As

¹SETI Institute, Mountain View, California, USA.

²NASA Ames Research Center, Moffett Field, California, USA.

³Department of Physics and Astronomy, Northern Arizona University, Flagstaff, Arizona, USA.

⁴Indian Institute of Technology, Kanpur, India.

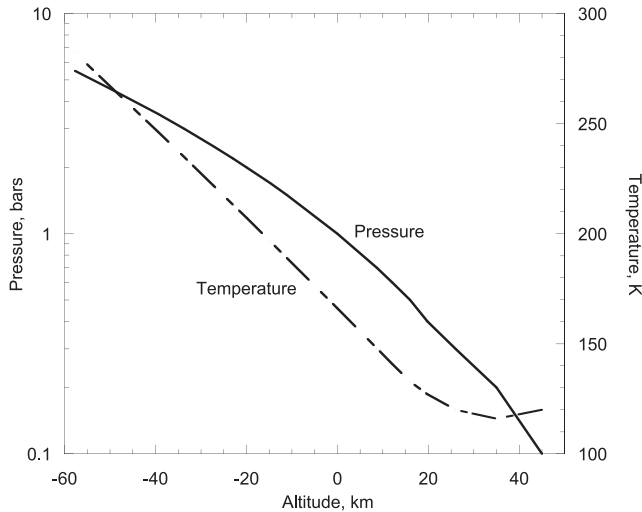


Figure 1. Atmospheric pressure and temperature as functions of altitude from *Seiff et al.* [1998].

Borucki and Whitten [2008] show, that process was completely negligible for the Titan haze particles observed by *Tomasko et al.* [2005], and we expect it to be similarly negligible for Jupiter.

[5] In this paper we report predictions of electron and ion concentrations, charge distributions on the cloud particles and the atmospheric electrical conductivities due to electrons and ions. We find that the clouds act as large reservoirs for negative charge because of the rapid attachment of electrons and the large total surface area of the particles. As a result of large uncertainties in many of the parameters such as cloud densities and particles sizes and shapes and reaction rates, our results are characterized by substantial uncertainties. Nevertheless, they provide valid order-of-magnitude estimates that can guide planning for future probe missions that seek to measure atmosphere and cloud electrical properties.

2. Atmospheric Environment and Cloud Properties

[6] Pertinent parts of the model atmosphere of *Seiff et al.* [1998] that are based on results obtained from the Galileo probe. Since the probe entered a hot spot in the North Equatorial Belt, atmospheric properties for the midlatitude region may be slightly different. However, because of other, greater uncertainties, especially cloud properties, the use of the *Seiff et al.* model is adequate for this study. We note that following *Seiff et al.* [1998], altitude zero is taken to coincide with 1.0 bar atmospheric pressure. The variation of pressure and temperature with altitude is illustrated in Figure 1. Methane is also present with a mixing ratio of about 2×10^{-3} [*Niemann et al.*, 1996]. As discussed above, methane, ammonia, and various hydrocarbon minor constituents are important in attenuating solar ultraviolet radiation that might cause photoemission of electrons from cloud particles.

[7] Using observations from the Voyager spacecraft, *Atreya and Wong* [2005] assumed steady state conditions and employed thermodynamic principles to compute cloud

masses for three cloud layers, the upper composed of NH_3 ice, the intermediate composed of NH_4SH ice and the lowest of water ice. Cloud number density distributions are shown in Figure 2.

[8] We have terminated our computations at 5.5 bars (-58 km altitude) because this region contains Jupiter's three major cloud regimes and the existence of deeper water-ammonia cloud is questionable. The particle densities that correspond to the sizes are as follows [from *West et al.*, 2004]:

$$\text{NH}_3 \text{ ice} - 0.7 \mu, \text{NH}_4\text{SH ice} - 1.2 \mu, \text{H}_2\text{O} - 5.0 \mu$$

3. Ion Production by Galactic Cosmic Rays

[9] Atmospheric ionization by galactic cosmic rays has been investigated extensively by one of the authors [*O'Brien*, 1969, 1970, 1971, 1972, 1975a, 1975b, 2005; *O'Brien et al.*, 1996]. For brevity only the results of the computations are presented here for system III latitudes 30° , 45° , and 60° and longitude 90° in Figures 3a and Figures 3b. Details of the computational method are presented in Appendix A. The effect of Jupiter's magnetic dipole tilt of 10° was included in the calculation.

[10] The computed ionization rates for GCR at three system III latitudes and 90° longitude are illustrated in Figures 3a (solar minimum) and 3b (solar maximum). Note that the ionization profiles for solar minimum and maximum are sufficiently close that only solar minimum will be used in the computations of electron and ion abundances and particle charge distributions. Also, ionization of H_2 and He are combined within the program.

[11] In the following work we have assumed that the positive ions created by GCR ionization are H_2^+ (mass = 2 amu) and He^+ (mass = 4 amu). These ions undergo series of reactions with neutral atmospheric molecules, yielding heavy ions with masses approaching 100 amu. The chemistry that results in the formation of these ions is discussed in Appendix B. In order to assess the effect of the uncer-

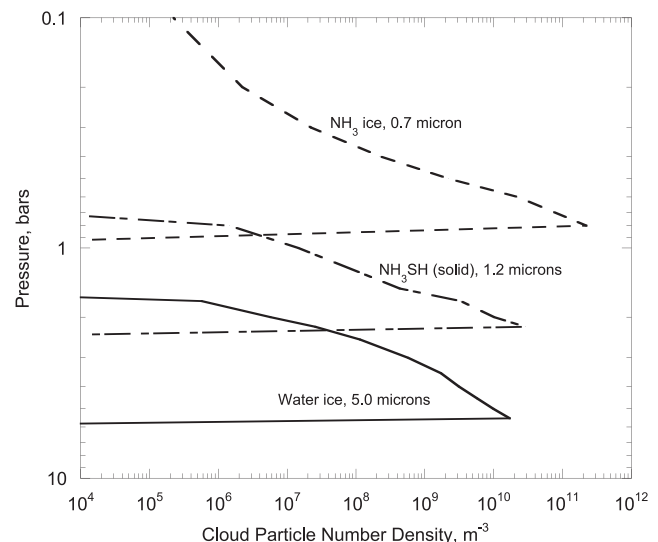


Figure 2. Cloud density distributions.

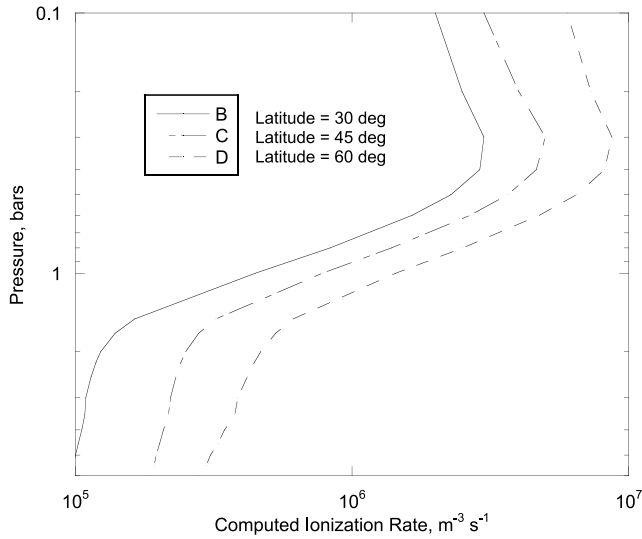


Figure 3a. Combined ionization rates of hydrogen and helium at 30°, 45°, and 60° latitude and longitude 90°, solar minimum.

tainty in ion masses, we performed computations of electron and ion abundances for both small and large ion masses. The results show little sensitivity to the assumed masses and are discussed later. Ion and electron mobilities and diffusivities for the heavy ions are presented in Appendix D. Negative ions, discussed in Appendix C, are not likely to be important because of the apparent absence of electron attaching species in sufficient abundance and because electron attachment to the cloud particles alone reduces the electron abundances to very low values.

4. Computational Method

[12] Our model of the electrical charging of the aerosol particles is nearly identical to that discussed in an earlier paper on Titan [Borucki *et al.*, 2006]. Briefly stated, it is based on the work of Natanson [1960], Parthasarathy [1976] and especially Jensen and Thomas [1991].

[13] The rate equations for the electron and positive ion densities at each altitude are

$$\frac{dn_e}{dt} = Q - \{\alpha_1 + \alpha_2([H_2] + [He])\}n_en_+ - d_en_e \quad (1)$$

$$\frac{dn_+}{dt} = Q - \{\alpha_1 + \alpha_2([H_2] + [He])\}n_en_+ - d_+n_+ \quad (2)$$

The requirement that every volume of space be electrically neutral imposes the condition;

$$zp + n_+ - n_e = 0 \quad (3)$$

where zp is the charge on the aerosol particles, given by

$$zp = \sum_{i,p} pN_{i,p} \quad (4)$$

Here,

- Q molecular ionization rate ($m^{-3} s^{-1}$) due to energetic particle radiation;
- α_1 electron-positive ion dissociative recombination coefficient;
- α_2 pressure-dependent electron-positive ion three-body recombination coefficient ($m^3 s^{-1}$);
- d_e combined diffusion/effusion rate of electrons to aerosol particles (s^{-1});
- d_+ combined diffusion/effusion rate of positive ions (s^{-1}) to aerosol particles;
- n_e electron density (m^{-3});
- n_+ positive ion density (m^{-3});
- N total number density of aerosols (m^{-3});
- $N_{i,p}$ number density of aerosols in size bin “ i ” and with charge state “ p ”;
- zp total charge on the aerosols with sign (m^{-3}).

[14] The reduction of ions and electrons due to the presence of the aerosols is calculated by the method described by Borucki *et al.* [2006]:

$$N_{i,p}\nu_p^{i,+}n_+ + N_{i,p}\nu_p^{i,e}n_e = N_{i,p+1}\nu_{p+1}^{i,e}n_e + N_{i,p-1}\nu_{p-1}^{i,+}n_+ \quad (5)$$

where $N_{i,p}$ is the fractional concentration of aerosol particles with size “ i ” and charge “ p ,” $\nu_p^{i,e}$ is the capture rate coefficient for electrons by particles with charge p ($m^3 s^{-1}$), and $\nu_p^{i,+}$ is the capture rate coefficient for positive ions by aerosols with charge p ($m^3 s^{-1}$). The “ ν ” are dependent upon the aerosol particle radius (size mode) as well as charge. The solution of the charge balance equations under steady state conditions has been described in detail by Borucki *et al.* [2006] and is not repeated here.

[15] The positive ion-electron dissociative recombination coefficient α_1 is taken as $4.0 \times 10^{-12} m^3 s^{-1}$ [Mitchell, 1990]. This is a typical value for dissociative recombination coefficients for positive ions with some clustering with

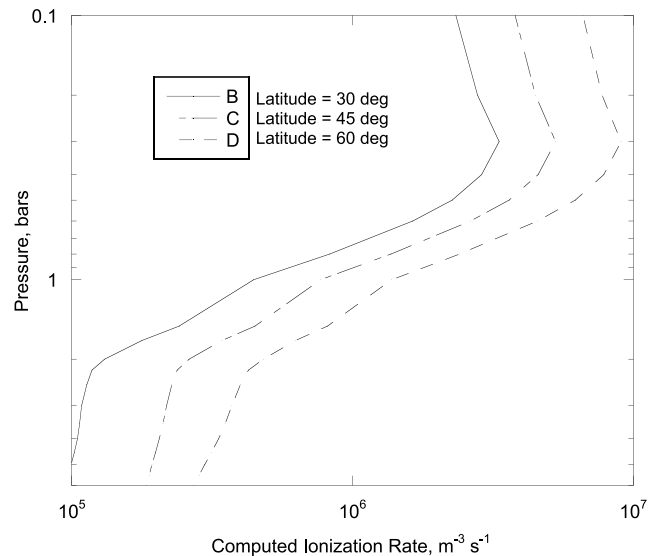


Figure 3b. Combined ionization rates of hydrogen and helium at 30°, 45°, and 60° latitude and longitude 90°, solar maximum.

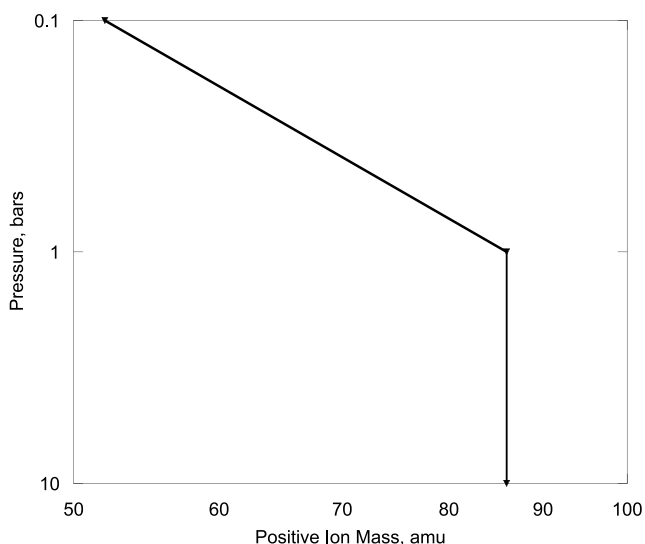


Figure 4. Variation of large ion mass with altitude (see Appendix B for discussion).

neutral molecules [Banks and Kockarts, 1973]; α_2 is the pressure-dependent three-body recombination cross section for electrons with positive ions and positively charged embryos and is given by

$$\alpha_2 = 2 \times 10^{-37} (300/T)^{2.5} \times ([H_2] + [He]) \text{ m}^3 \text{ s}^{-1} \quad (6)$$

It is important at high pressure and is consistent with that from Smith and Church [1977]. Here T is the absolute atmospheric temperature in kelvins, and H_2 and He are the hydrogen and helium number densities, respectively, in m^{-3} .

5. Results

[16] In order to learn if the formation of heavy positive ions by reaction with various hydrocarbon and ammonia

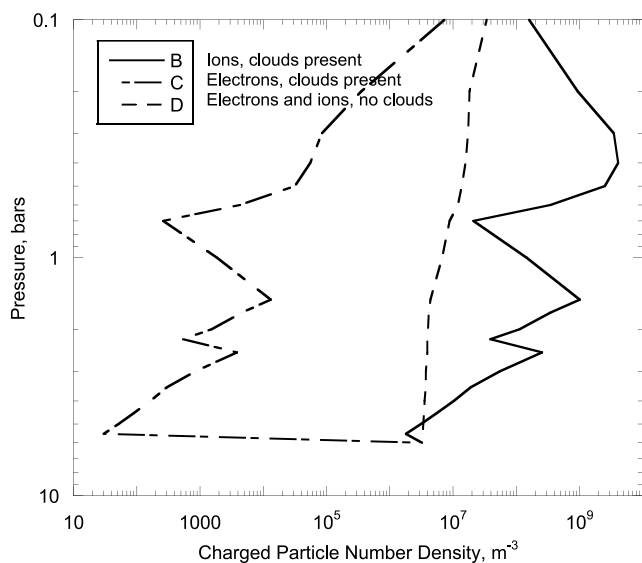


Figure 5. Electron and ion densities without clouds present, 60° latitude, 90° longitude, solar minimum. Large mass positive ions (Figure 4).

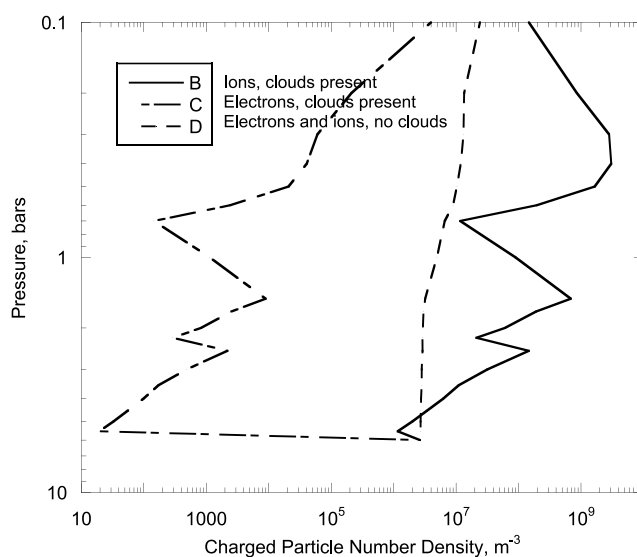


Figure 6. Electron and ion densities without clouds present, 45° latitude, 90° longitude, solar minimum. Large mass positive ions (Figure 4).

molecules affects the ion and electron abundances, we performed computations for two cases of positive ion masses: one varying between 86 and 52 amu, pressure-/altitude-dependent as illustrated in Figure 4 and discussed in Appendix B, and a second for light ions of mass 12 amu. The corresponding electron and ion abundances for heavy ions at solar minimum are shown in Figures 5, 6, and 7. Although the influence of the presence of the aerosols is quite evident, there is little dependence on latitude. Figure 8 shows the computed electron and ion abundances at 45° latitude for small ion mass (12 amu). The electron abundances do not differ at all and the ion abundances differ by a factor of at most about two from the ion profile shown in Figure 6, suggesting that electron and ion abundances are

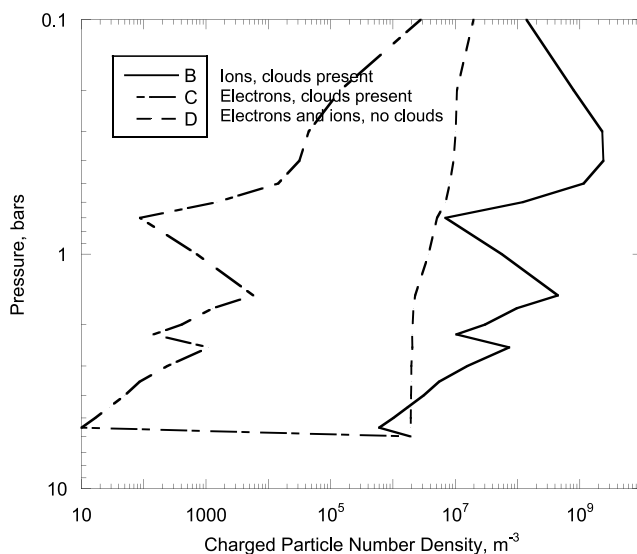


Figure 7. Electron and ion densities without clouds present, 30° latitude, 90° longitude, solar minimum. Large mass positive ions (Figure 4).

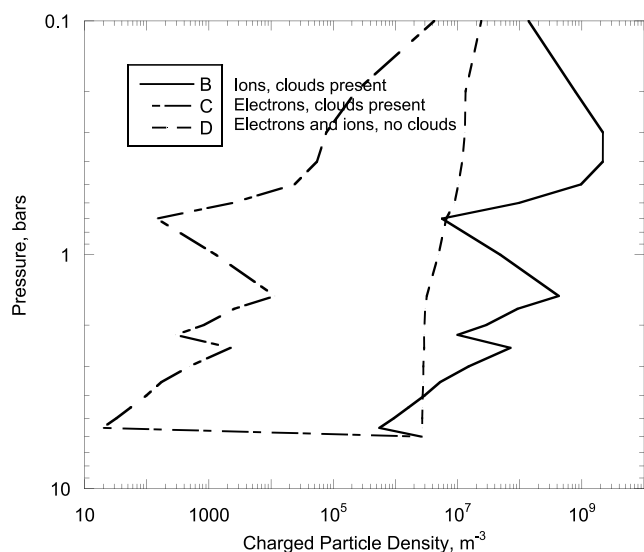


Figure 8. Electron and ion densities without clouds present, 45° latitude, 90° longitude, solar minimum. Small mass positive ions (12 amu).

not very sensitive to ion mass and that any mass departures from Figure 4 will not cause significant error. Figures 5 through 8 also show the electron and ion abundances for the case of no clouds present. The profiles with no clouds present assume that electrophilic species are negligible and negative ions can be ignored. See Appendix C for a discussion of negative ions for both clouds present and clouds absent.

[17] The striking feature of the influence of the clouds as negative charge reservoirs is the very low number density of electrons at all atmospheric pressures included in this study 5.5 to 0.1 bars (-58 to 45 km altitude). Electron densities are reduced by interaction with the cloud particles at all altitudes included in our computations. Thus the clouds serve as reservoirs for most of the negative charge by many orders of magnitude. Ion densities, on the other hand, are larger at all pressure/altitudes above 5.5 bars (-58 km altitude) than would be the case in the absence clouds. The increase in ion density is due to the much reduced rate of recombination with electrons. Migration of positive ions to the cloud particles is a relatively slow loss mechanism but, as will be shown later, does result in some positive charging of cloud particles. Since we terminate the lower cloud layer at 5.5 bars, the electron and ion abundances at 6.0 bars converge to the “no cloud” case, which is apparent in Figures 5 to 8. At 5.5 bars the loss of positive ions by collision with negatively charged particles is sufficient to reduce the ion number density below the value for no clouds present. While the ion number density profiles generally do not fall below the values for a clear atmosphere, they do show sharp decreases in the vicinity of the cloud particle maxima.

[18] Figures 9 through 11 illustrate the charge distributions on the aerosol particles at latitude 60° . For the lowest cloud layer, Figure 9 shows that the distribution peaks occur at a positive charge of about $+6$. However, the mean charge is negative as evidenced by the skewed shapes of the curves. The mean net negative charge per particle is very small

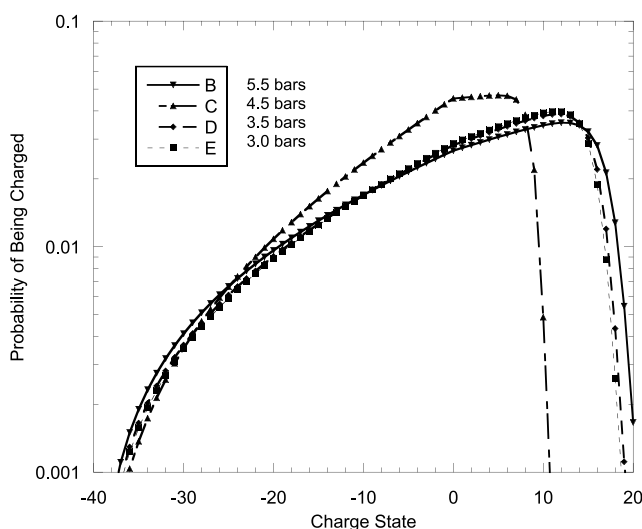


Figure 9. Charge distributions on lower cloud layer $-5.0 \mu\text{m}$ aerosol particles.

(about 10^{-3}). However, the very large abundance of cloud particles (about 10^{10} m^{-3} at 5 bars) results in a total negative charge on the cloud particles of 10^7 m^{-3} while the abundance of free electrons shown in Figure 5 is only 30 m^{-3} . Figure 10 shows a somewhat similar behavior. However, Figure 11 shows that while the charge distributions are centered on small negative charges for pressures of 0.6 and 0.4 bar, they shift toward larger negative charges for lower pressures of 0.3 and 0.2 bar. The reason for the shift is twofold: (1) larger electron abundances at the lower pressures (0.2 and 0.3 bar) and (2) a smaller number density of cloud particles. Thus there are more electrons per cloud particle for attachment to the particles.

[19] Table 1 presents the mean particle charge for each cloud layer. The mean particle charge on the cloud particles is negative for all altitudes except for the lower cloud level

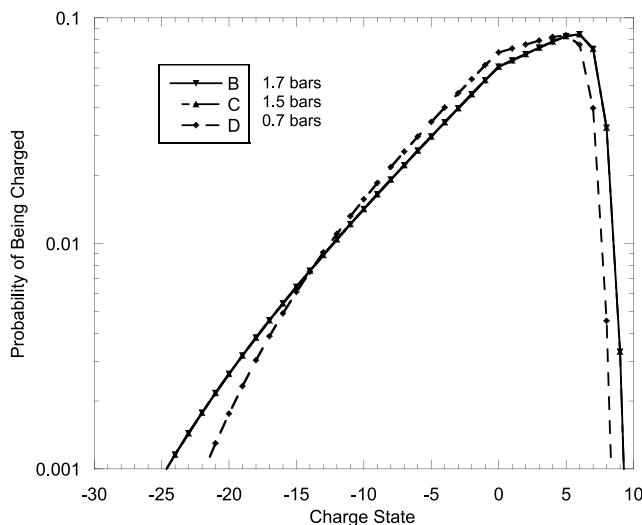


Figure 10. Charge distributions on middle cloud layer aerosol $-1.2 \mu\text{m}$ particles. The charge distributions at 1.5 and 1.7 bars nearly coincide.

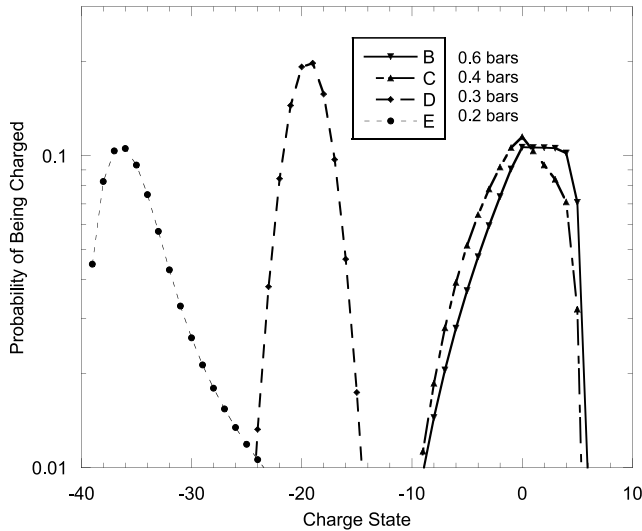


Figure 11. Charge distributions on upper cloud layer $-0.25 \mu\text{m}$ aerosol particles.

(radius = $5.0 \mu\text{m}$) in the range 2.20 to 1.7 bars (-23.0 to -14.8 km) where the mean charge on the lower cloud particles (radius = $5.0 \mu\text{m}$) is positive. These charge states can be explained by the very low electron abundance caused by electron attachment to the particles and large ion abundance in that pressure range. Migration of ions to the particles is sufficiently fast compared to that of electrons that the particles experience a buildup of positive charge on the particles. At this altitude, the sum of the cloud particles when summed over both the middle and lower cloud layer is negative as expected from charge conservation.

[20] Figure 12 shows the loss rates for the ions. When clouds are present the dominant loss mechanism at all pressure altitudes is neutralization by negatively charged particles as opposed to electron recombination. Even in the few instances when mean particle charge is positive there are still large quantities of negatively charged particles for

Table 1. Mean Charge on Cloud Particles

Altitude, km	Pressure, bars	High Cloud Mean Charge	Middle Cloud Mean Charge	Low Cloud Mean Charge
-62.0	6.0	0.0000E+00 ^a	0.0000E+00	-8.7600E+00
-57.7	5.5	0.0000E+00	0.0000E+00	-8.3860E-07
-54.0	5.0	0.0000E+00	0.0000E+00	-2.5220E-06
-49.4	4.5	0.0000E+00	0.0000E+00	-7.7390E-06
-45.0	4.0	0.0000E+00	0.0000E+00	-2.6210E-05
-39.4	3.5	0.0000E+00	0.0000E+00	-8.9350E-05
-33.7	3.0	0.0000E+00	0.0000E+00	-7.7570E-04
-27.3	2.5	0.0000E+00	0.0000E+00	-1.7970E-02
-23.0	2.2	0.0000E+00	-4.0910E-02	5.1530E+00
-19.9	2.0	0.0000E+00	-2.6150E-02	5.0130E+00
-14.8	1.7	0.0000E+00	-1.4660E-02	4.6850E+00
-11.1	1.5	0.0000E+00	-1.6860E-01	0.0000E+00
0.0	1.0	0.0000E+00	-2.8392E-01	0.0000E+00
8.7	0.7	-2.3570E-06	-4.7810E-01	0.0000E+00
12.1	0.6	-7.1940E-04	0.0000E+00	0.0000E+00
16.0	0.5	-5.1900E-02	0.0000E+00	0.0000E+00
19.8	0.4	-8.4400E-01	0.0000E+00	0.0000E+00
26.0	0.3	-7.2240E+00	0.0000E+00	0.0000E+00
35.0	0.2	-1.9390E+01	0.0000E+00	0.0000E+00
45.0	0.1	-3.1390E+01	0.0000E+00	0.0000E+00

^aRead 0.0000E+00 as 0.0000×10 .

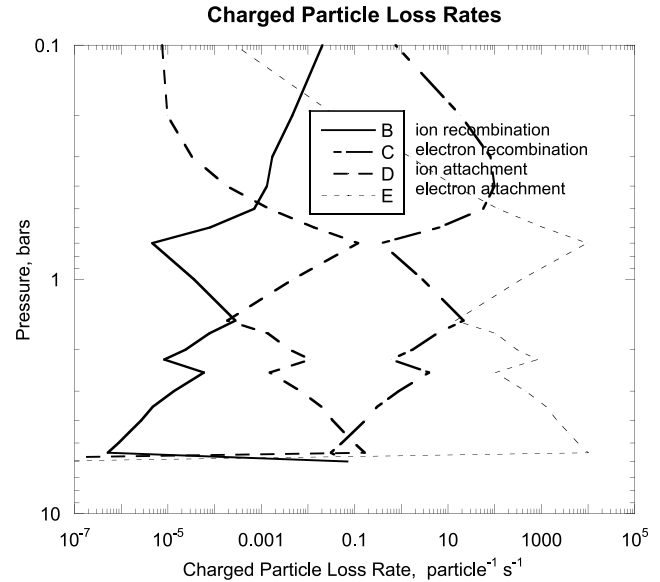


Figure 12. Ion loss rates (per particle per second) due to electron recombination and neutralization by negatively charged cloud particles, 45° latitude, 90° longitude, solar minimum.

neutralization of the positive ions. It is emphasized that these rates in s^{-1} are not fluxes of charged particles. To check that the rates are physically correct, we multiplied the ion capture rates by the ion abundances and the electron capture rates by the electron abundances. They should be equal and it proved to be so.

[21] An examination of Figure 13 shows that the electron and ion conductivities are nearly identical for pressures greater than 0.5 bar. This occurs in the diffusion (high pressure range) when the recombination of electrons and ions on the aerosols dominates the molecular ion-electron recombination. For these conditions, the diffusion-dominated ion and electron currents to the aerosols are approximately equal and

$$n_+ D_+ = n_e D_e \quad (7)$$

where n^+ is the abundance of positive ions, D^+ is the diffusivity of positive ions, n_e is the abundance of electrons, and D_e is the diffusivity of electrons.

[22] However,

$$D = KkT/e \quad (8)$$

where K is the mobility, k is the Boltzmann constant, T is the temperature, and e is the electron charge [McDaniel and Mason, 1973]. Substituting equation (8) into equation (7) and noting that the equations for electron and positive ion conductivity are

$$\sigma_e = eK_e n_e \quad (9a)$$

$$\sigma_+ = eK_+ n_+ \quad (9b)$$

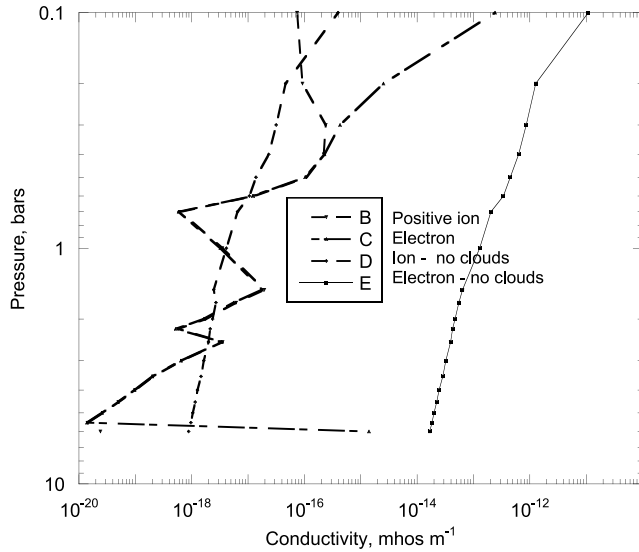


Figure 13. Electron and ion conductivity, 60° latitude, 90° longitude, solar minimum.

we see that the equality in equation (7) explains the nearly identical variation of the electron and ion conductivities with altitude for the lower part of the atmosphere.

[23] Mobilities for hydrogen and helium were taken from *Ramanan and Freeman* [1990, 1991] and ion mobilities from *Meyerott et al.* [1980], who obtained an approximate expression from laboratory measurements. We have modified some of the constants to reflect the units used in this paper to obtain

$$K_+ = 5.05 \times 10^{21} (83.0/\text{ion mass})^{0.376} / N_{\text{atm}} \quad (10)$$

where ion mass is the mean positive ion mass and N_{atm} is the atmospheric number density. Values of electron and positive ion mobilities and diffusivities are tabulated in Appendix D.

6. Conclusions

[24] 1. The presence of cloud particles at and above the 5.5 bar pressure level reduces electron densities at all pressures considered here. While most of the negative charge resides on the cloud particles, the positive charge is not attached as effectively. Positive ion densities are, however, increased at all pressures except 5.5 bars (−59.7 km altitude) by the presence of clouds.

[25] 2. At most atmospheric pressures greater than 2.2 bars (−23 km altitude), the charge on the low cloud particles is slightly negative as a result of the high concentrations (and total surface area) of the particles. At atmospheric pressures of 2.2 bars and less, the mean charge on the lower cloud particles becomes slightly positive. The charge on the middle and upper cloud particles is negative.

[26] 3. The electron conductivity is predicted to be sufficiently high that it could be measured with a relaxation probe with capabilities similar to that employed on the Huygens entry probe [*Grard et al.*, 1995] only for pressures below 0.2 bar.

[27] 4. Ion clustering has little influence on the electron abundances but does affect the ion abundances because of the ion concentration dependence on ion diffusivity.

[28] 5. Negative ions are not likely to be significant in the altitude/pressure region in which clouds are present but may be so above and below this region.

Appendix A: Ionization by Galactic Cosmic Rays

[29] Solar wind interacts with the cosmic particles in the interplanetary medium and its variations related to the solar activity produce changes in the spectrum of cosmic rays. This modulation can be approximated by a heliocentric electric potential [*Gleeson and Axford*, 1967].

[30] *Caballero-Lopez and Moraal* [2004] show that the heliocentric potential approximation is valid out to approximately 20 AU. Its dependence on the distance from the solar wind transition is given by

$$U = \frac{1}{3} V \frac{(r_s - r)}{\kappa_0} \quad (A1)$$

where U is the heliocentric potential in MV, V is the solar wind velocity, taken as a constant 400 km s^{−1}, r is the distance in km at which the potential is to be evaluated from the sun as origin, r_s is the distance of the solar wind transition from the sun and κ_0 is obtained from the scalar diffusion coefficient, $\kappa = \kappa_0 P \beta$, again where P is the particle rigidity and $\beta = v/c$ is the particle velocity, v , relative to the velocity of light, c . Thus one can see that the heliocentric potential at the distance of Jupiter is 95% of the value at Earth, where it was, of necessity determined. We use 466 MV, determined at the last solar minimum, and 1300 MV determined at the last solar maximum, reduced by 5% to characterize solar minimum and solar maximum at Jupiter.

[31] The heliocentric potential at 1 AU is determined from the counting rate of high-latitude neutron monitors [*O'Brien*, 2005].

[32] Figure A1 shows the cosmic ray differential energy spectra for solar modulation parameters of 400, 600 and 1000 MV. The variations from each other are significant only at energies below ∼1 GeV.

[33] Cosmic rays are propagated through the atmosphere by means of nucleonic cascade and are assumed to be isotropic downward. The primary nuclei impact the atmospheric molecules producing secondary nuclei, nucleons and pions; neutral pions quickly decay to gamma rays, which interact with the atmosphere through the electromagnetic cascade while charged pions decay to muons, which do not strongly interact with the atmosphere. They decay into an electron/positron plus two neutrinos with enough energy to initiate an effective electromagnetic shower [*O'Brien*, 2005].

[34] We have adapted the *O'Brien* [2005] code, initially written for the Earth's atmosphere, to the conditions of Jupiter in order to calculate the production rate of ions. The mathematical treatment for cosmic ray transport is described in detail in that reference.

[35] Since the incoming particles that interact with the atmosphere of Jupiter have energies largely above 100 MeV, the cross sections used were geometric (equal to the size of the nucleus) and constant with energy [*Barashenkov et al.*,

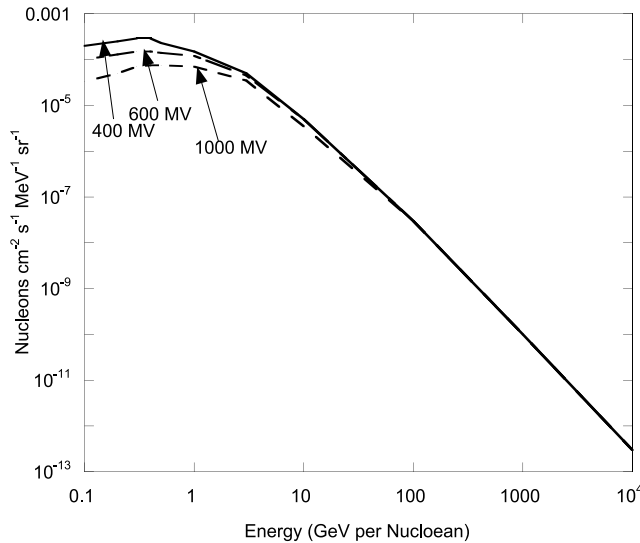


Figure A1. Galactic cosmic ray spectra as function of heliocentric potential.

1968]. The stopping powers were taken from *O'Brien* [1972]. The production spectra were derived from a combination of experimental and theoretical models [*O'Brien*, 1971, 1975a, 2005].

[36] The propagation of the electromagnetic cascade is treated in a very simple way. Electromagnetic showers are produced by two mechanisms.

[37] 1. Photons are produced by the production of neutral pions. Neutral pions have a mean life of 8.4×10^{-17} s and decay almost immediately into two photons creating an electromagnetic shower with a total energy comprising the rest mass of the neutral pion (produced in the hadron collision process) and its kinetic energy.

[38] 2. Muons have a $2\text{-}\mu\text{s}$ mean life, decaying into a neutrino-antineutrino pair and an electron/positron. This decay is treated in detail. The energy deposition from charged pion decay is calculated by assuming that the total energy of the pion and one third of the energy of the decaying muon is given to the electron, also creating an electromagnetic shower. The energy taken up by electromagnetic showers is deposited at the point of production. Charged pions decay with a mean life of 26 ns.

[39] Another important contribution to ionization is provided by the continuous slowing down of charged particles, muons, charged pions and protons. At high altitude levels, the maximum of the ion production rate is due to the production of secondary particles (nuclei, hadrons, leptons and photons) by hadron-nucleus and nucleus-nucleus collisions. As the penetration depth increases, energy is drained from the cascade and the ionization rate decreases approximately exponentially with increasing depth.

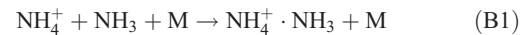
[40] The minimal interaction of muons with the atmospheric constituents and their relatively long lifetime (2×10^{-6} s versus 8.4×10^{-17} s and 2.551×10^{-8} s, for π^0 and π^{\pm} , respectively [*O'Brien et al.*, 1996]) implies that muons can penetrate down to larger depths and deposit

their energy below the levels where the other ionization sources peak.

Appendix B: Cluster Ions in Jovian Atmosphere Formation of Positive Secondary Ions and Ion Clusters

[41] In the Jovian atmosphere (from 10 bars to 1 mbar) muon flux component of galactic cosmic rays are the main ionization source as explained in section 3. They penetrate to the deep atmosphere at levels where the total number density exceeds 10^{25} m^{-3} and ionize the neutral constituents (mainly H_2 and He as well as CH_4 , NH_3), producing the primary ions H_2^+ , He^+ , CH_4^+ , CH_3^+ , CH_2^+ and electrons. Fast reactions with the neutrals rapidly convert these into secondary ions and ion clusters. Studies of stratospheric conductivity on Earth suggest that less mobile but relatively long-lived molecular cluster ions provide the main contribution to the stratospheric conductivity [*Hua and Holzworth*, 1996]. The He^+ ions that are initially formed also get converted into CH_5^+ due to abundance of H_2 and CH_4 and the inverse temperature dependence of three-body association reaction [*Hiraoka and Kebarle*, 1975]. Bimolecular reactions of CH_5^+ ions with the most abundant species H_2 , He and CH_4 are not possible [*Capone et al.*, 1979], but CH_5^+ reacts with C_2H_6 and NH_3 to produce C_2H_7^+ and NH_4^+ , respectively. At altitudes near and above the ionization peak where concentration of ammonia decreases very rapidly with altitude, bimolecular ion-molecule reactions are no longer important loss processes for these ions; instead three-body ion cluster reactions play a major role [*Capone et al.*, 1979].

[42] After considering various possible ion clustering reactions in lower atmosphere of Jupiter such as H_3^+ with H_2 , NH_4^+ with NH_3 and CH_5^+ with CH_4 , we find that clustering of ions H_3^+ with H_2 becomes relatively unimportant due to small lifetime of H_3^+ and lower rate constant of this reaction. The formation of the cluster between NH_4^+ and NH_3 controls the loss process of NH_4^+ in the lower deep troposphere of Jupiter. In the absence of laboratory data for clustering of ions to CH_4 and NH_3 , *Capone et al.* [1979] assumed three rate coefficients, 0 , 10^{-31} , and $10^{-29} \text{ cm}^6 \text{ s}^{-1}$ to predict the cluster ion concentration. Under the first condition NH_4^+ was found to be most dominant positive ion with hydrocarbon ions becoming more prevalent above the ionization peak. However, in later two cases $\text{NH}_4^+ \cdot \text{NH}_3$ became increasingly more dominant with increasing rate coefficient. More recently, *Hamon et al.* [2002] measured the association reaction rate with a coefficient of $2.34 \times 10^{-41} (300/T)^{-3.38} \text{ m}^6 \text{ s}^{-1}$. Therefore equilibrium between the molecular cluster and cation is established



[43] At equilibrium, the cluster ion $\text{NH}_4^+ \cdot (\text{NH}_3)_n$ is expected to be dominated by the size $n = 4$ between 10 bars to 1 bar and decreases to size $n = 2$ at 100 mbar due to increasing temperature and decreasing ammonia concentration.

[44] Because of relatively low temperature expected in this region of the Jovian atmosphere, collisional destruction of the ion clusters is unimportant [*Capone et al.*, 1979]. Moreover, because of very dense atmosphere and large

Table B1. Calculated Values of the Mass of the Ion Clusters in Jupiter's Atmosphere

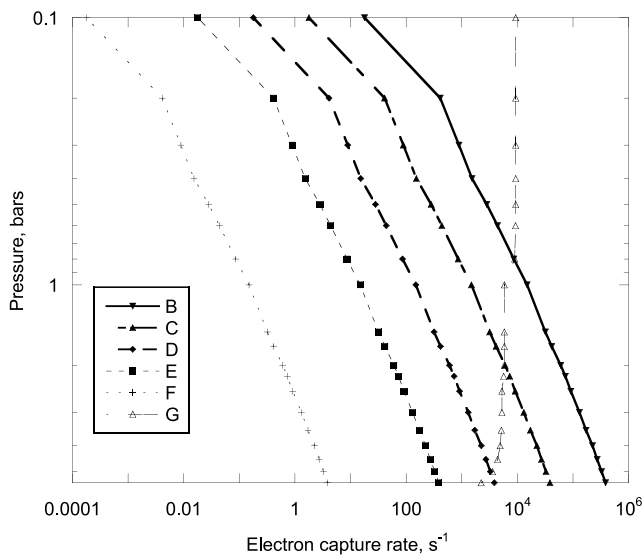
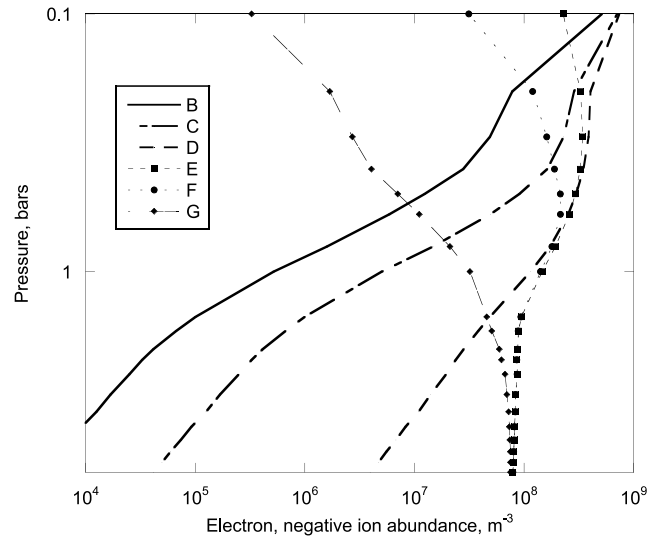
Pressure, bars	Type of Positive Ion Cluster	Mass, amu
10	$\text{NH}_4^+ \cdot (\text{NH}_3)_4$	86
1	$\text{NH}_4^+ \cdot (\text{NH}_3)_4$	86
0.1	$\text{NH}_4^+ \cdot (\text{NH}_3)_2$	52

Jupiter-Sun distance, photodissociation of the cluster ions also becomes unimportant and ion clustering predominates in this region of the Jovian atmosphere. Calculated values of the mass of the ion clusters in Jupiter's atmosphere are shown in Table B1.

Appendix C: Negative Ions

[45] As suggested in the foregoing, electrophillic species probably occur in the Jovian atmosphere, e.g., NH_2 , CH_3 , OH . The question, however, is are they present in sufficient abundance to influence (1) the electrical charging of the cloud particles and (2) those parts of the atmosphere in which no cloud particles are present? To resolve the first question, we assumed the presence of a well mixed electrophillic constituent such as O_2 in various mixing ratios as shown in Figure C1. Minor constituents such as NH_2 , CH_3 , OH are very chemically active and will not likely be present in mixing ratios of the order of 1 part per million (ppm). A constituent that would be present in sufficient abundance to compete with the cloud particles in attaching electrons would have to be chemically inactive, e.g., O_2 , and present in mixing ratios of at least 1 ppm. We have no evidence from past observations for the presence of such a constituent in sufficient quantities to be significant.

[46] In order to obtain the electron attachment rates illustrated in Figure C1 for case 1, we employed a simple model of the Jovian ionosphere to compute the electron, positive ion and negative ion abundances and the rate of

**Figure C1.** Electron capture rates, latitude 45° , longitude 90° , large ion mass clustering. The profiles correspond to the following mixing ratios of attaching species: profiles B, 10^{-4} ; C, 10^{-5} ; D, 10^{-6} ; E, 10^{-7} ; and F, 10^{-9} .**Figure C2.** Electron and negative ion density, latitude 45° , longitude 90° , clouds not present. Profiles B, C, and D refer to electrons, profiles E and F refer to negative ions. The profiles correspond to the following mixing ratios of attaching species: profiles B, 10^{-8} ; C, 10^{-9} ; D, 10^{-11} ; E, 10^{-8} ; and F, 10^{-9} . Large ion mass clustering.

negative ion formation by attachment of electrons to the assumed electrophillic species by assuming that the presence of the cloud particles did not affect the rates. The total electron capture rate for the densities shown in Figure 2 is illustrated for comparison.

[47] The positive ion–negative ion recombination was taken to be the same as the three-body positive ion–electron coefficient while the three-body electron attachment rate was taken from *Banks and Kockarts [1973]*:

$$\kappa = 1.5 \times 10^{-41} (300/T) \exp(-600/T) \text{ m}^6 \text{ s}^{-1} \quad (\text{C1})$$

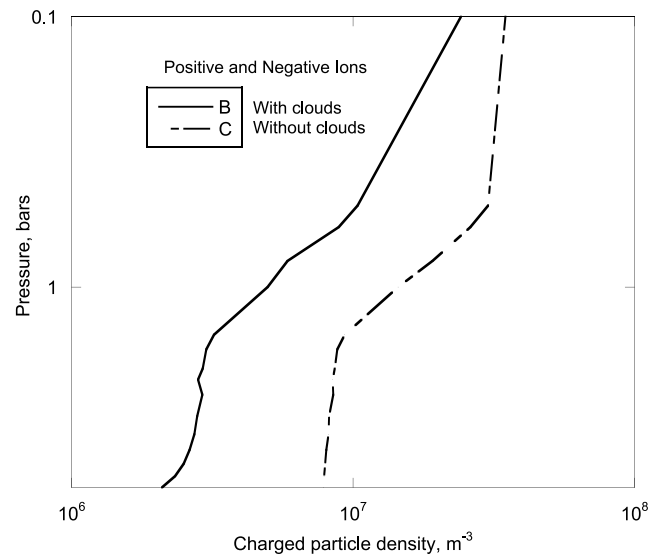
**Figure C3.** Ion density 45° , longitude 90° , large ion mass clustering.

Table D1. Electron and Positive Ion Mobilities and Diffusivities

Pressure, bars	Ion Mobility, $\text{m}^2 \text{V}^{-1} \text{s}^{-1}$	Electron Mobility, $\text{m}^2 \text{V}^{-1} \text{s}^{-1}$	Ion Diffusivity, $\text{m}^2 \text{s}^{-1}$	Electron Diffusivity, $\text{m}^2 \text{s}^{-1}$
6.00	5.8300E-07	1.1000E-02	1.4600E-08	2.7500E-04
5.50	6.2200E-07	1.1800E-02	1.5100E-08	2.8600E-04
5.00	6.6200E-07	1.2600E-02	1.5700E-08	2.9800E-04
4.50	7.1200E-07	1.3600E-02	1.6300E-08	3.1200E-04
4.00	7.6600E-07	1.4800E-02	1.7000E-08	3.2700E-04
3.50	8.5000E-07	1.6500E-02	1.8000E-08	3.5000E-04
3.00	9.4400E-07	1.8500E-02	1.9100E-08	3.7500E-04
2.50	1.0900E-06	2.1400E-02	2.1000E-08	4.1500E-04
2.20	1.1600E-06	2.3200E-02	2.1400E-08	4.2700E-04
2.00	1.2500E-06	2.5000E-02	2.2300E-08	4.4700E-04
1.70	1.4000E-06	2.8400E-02	2.3200E-08	4.7200E-04
1.50	1.2000E-06	3.1200E-02	1.9100E-08	4.9600E-04
1.00	1.3200E-06	4.0900E-02	1.8900E-08	5.8600E-04
0.80	1.5700E-06	4.9300E-02	2.0900E-08	6.5700E-04
0.60	1.9100E-06	6.0900E-02	2.3200E-08	7.4000E-04
0.50	2.1600E-06	6.9700E-02	2.4700E-08	7.9800E-04
0.40	3.1700E-06	8.5700E-02	3.4200E-08	9.2400E-04
0.30	3.9000E-06	1.0600E-01	4.0700E-08	1.1000E-03
0.20	5.4600E-06	1.4900E-01	5.5600E-08	1.5200E-03
0.10	2.4800E-05	6.8000E-01	2.4600E-07	6.7400E-03

This equation is strictly true only when molecular oxygen is the third body since the reaction



is a resonant process and thus larger than would be the case if the third body is some other species such as molecular hydrogen. Hence we reduced the numerical constant in equation (C1) from 1.5×10^{-41} to 1.5×10^{-42} for the computations reported here. Finally, we expect negative ions to form clusters as described for positive ions in Appendix B.

[48] Profile G in Figure C1 represents the computed total electron attachment rate to the cloud particles. Figure C1 shows that the mixing ratio of the electrophillic constituent must be 10^{-6} or larger to compete with and change the loss rate of electrons to the cloud particles. It also shows that even for such large densities, the effects will be significant only at the lowest altitudes.

[49] At pressures higher than about 6 bars clouds may be absent. For that case negative ions may become an important, even the predominant, carrier of negative charge. Figure C2 illustrates the computed electron and negative ion abundances for various mixing ratios of minor constituents if clouds are absent. Then mixing ratios of less than 1 part per billion are sufficient to influence the electron and negative ion abundance. For example, a mixing ratio as small as 10^{-11} causes the negative ion abundance to exceed the electron abundance at pressures greater than 1 bar. Mixing ratios of 10^{-9} and larger cause the negative ion abundance to exceed the electron abundance at all pressures greater than 0.1 bar.

[50] Figure C3 illustrates the computed positive and negative ion abundances if the attachment of electrons to electrophillic species is so fast that essentially all of the negative charge is in the form of negative ions. Here we have assumed that the mass of the clustered negative ions is equal to the mass of the clustered positive ions. Under these conditions, the net charge on the cloud particles is zero

because the mobilities of the two ion species are equal and thus diffuse to the cloud particles at the same rate. For the same reason the abundances of the two species are also equal. However, the interaction with the particles (charging and neutralizing) results in an increase in the effective ion recombination coefficient and thus smaller ion densities.

[51] To summarize the results of Appendix C, negative ions are very unlikely to be significant carriers of negative charge in the cloud region (~ 0.1 to 6 bars) but may be important above and below the cloud region.

Appendix D: Electron and Ion Mobilities and Diffusivities

[52] Table D1 presents the electron and positive ion mobilities and diffusivities for the ion masses in Figure 5.

[53] **Acknowledgments.** The authors wish to thank Richard Turco of the University of California, Los Angeles, and Robert Carlson of the Jet Propulsion Laboratory for helpful comments.

References

- Atreya, S. K., and A. S. Wong (2005), Coupled clouds and chemistry of the giant planets—A case for multiprobes, in *The Outer Planets and Their Moons*, edited by T. Encrenaz et al., pp. 121–136, Springer, New York.
- Banks, P. M., and G. Kockarts (1973), *Aeronomy, Part B*, pp. 257–260, 278, Academic, New York.
- Barashenkov, V. S., K. K. Gudima, and V. D. Toneeva (1968), Energy dependence of nuclear cross sections above 10 MeV, *Dubna Rep. P2-4183*, Jt. Inst. for Nucl. Res., Moscow.
- Borucki, W. J., and R. C. Whitten (2008), Influence of high abundances of aerosols on the electrical conductivity of the Titan Atmosphere, *Planet. Space Sci.*, 56, 19–26.
- Borucki, W. J., R. C. Whitten, E. L. O. Bakes, E. Barth, and S. Tripathi (2006), Predictions of the electrical charging of the aerosols in Titan's atmosphere, *Icarus*, 181, 527–544.
- Caballero-Lopez, R. A., and H. Moraal (2004), Limitations of the force-field equation to describe cosmic ray modulation, *J. Geophys. Res.*, 109, A01101, doi:10.1029/2003JA010098.
- Capone, L. A., J. Dubach, R. C. Whitten, and S. Prasad (1979), Cosmic ray ionization in the Jovian atmosphere, *Icarus*, 39, 433–449.
- Friedlander, S. K. (1977), *Smoke, Dust and Haze*, John Wiley, New York.
- Fuchs, N. A. (1961), *Aerosols*, Pergamon, London.

- Gleeson, L. J., and W. L. Axford (1967), Cosmic rays in the interplanetary medium, *Astrophys. J.*, *L149*, 116–118.
- Grard, R., et al. (1995), An experimental investigation of atmospheric electricity and lightning activity to be performed during the descent of the Huygens probe onto Titan, *J. Atmos. Terr. Phys.*, *57*, 575–578.
- Hamon, S., T. Speak, J. B. A. Mitchell, B. R. Rowe, and J. Troe (2002), Experimental and theoretical study of the ion-molecule association reaction $\text{NH}_4^+ + \text{NH}_3 + \text{M} = \text{N}_2\text{H}_7^+ + \text{M}$, *J. Chem. Phys.*, *117*(6), 2557–2567.
- Hiraoka, K., and P. Kebarle (1975), Temperature dependence of bimolecular ion molecule reactions: The reaction $\text{C}_2\text{H}_7^+ + \text{CH}_4 = \text{C}_3\text{H}_7^+ + \text{H}_2$, *J. Chem. Phys.*, *63*(1), 394–397.
- Hua, H., and R. H. Holzworth (1996), Observation and parameterization of the stratospheric electrical conductivity, *J. Geophys. Res.*, *101*, 29,539–29,552.
- Jensen, E. J., and G. E. Thomas (1991), Charging mesospheric particles: Implications for electron density and particle coagulation, *J. Geophys. Res.*, *96*, 18,603–18,615.
- Lellouch, E., B. Bézard, J. I. Moses, G. R. Davis, P. Drossart, H. Feuchtgruber, E. A. Bergin, R. Moreno, and T. Encrenaz (2002), The origin of water vapor and carbon dioxide in Jupiter's stratosphere, *Icarus*, *159*, 112–131.
- McDaniel, E. W., and A. E. Mason (1973), *The Mobility and Diffusion of Ions in Gases*, John Wiley, New York.
- Meyerott, R. E., J. B. Reagan, and R. G. Joiner (1980), The mobility and concentration of ions and the ionic conductivity in the lower ionosphere, *J. Geophys. Res.*, *85*, 1273–1278.
- Mitchell, J. B. A. (1990), The dissociative recombination of molecular ions, *Phys. Rep.*, *186*, 215–248.
- Natanson, G. L. (1960), On the theory of the charging of a microscopic aerosol particles as a result of capture of gas ions, *Zh. Tekh. Fiz.*, *30*, 573–588. (*Sov. Phys. Tech. Phys.*, *Engl. Transl.*, *5*, 538–551, 1960.)
- Niemann, H. B., et al. (1996), The Galileo probe mass spectrometer: Composition of Jupiter's atmosphere, *Science*, *272*, 846–849.
- O'Brien, K. (1969), Extra-nuclear hadron cascade calculations using Poisson's approximation, *Nucl. Instrum. Methods*, *72*, 93–98.
- O'Brien, K. (1970), Calculated cosmic ray ionization in the lower atmosphere, *J. Geophys. Res.*, *75*, 4357–4359.
- O'Brien, K. (1971), Cosmic-ray propagation in the atmosphere, *Nuovo Cimento A*, *3*, 52–78.
- O'Brien, K. (1972), Propagation of muons underground and the primary spectrum below 40 TeV, *Phys. Rev. D*, *5*, 591–605.
- O'Brien, K. (1975a), The cosmic ray field at ground level. Natural Radiation Environment II, *USERDA Rep. CONF-72085, Part 1*, pp. 15–54, U. S. Dep. of Commer., Natl. Tech. Inf. Serv., Springfield, Va.
- O'Brien, K. (1975b), Calculated cosmic-ray pion and proton fluxes at sea level, *J. Phys. A*, *8*, 1530–1534.
- O'Brien, K. (2005), The theory of cosmic-ray and high-energy solar particle transport in the atmosphere, in *The Natural Radiation Environment VII, Seventh International Symposium on the Natural Radiation Environment (NRE-VII)*, edited by J. P. McLaughlin, S. E. Simopoulos, and F. Steinhäusler, pp. 29–44, Elsevier, New York.
- O'Brien, K., W. Friedberg, H. H. Sauer, and D. F. Smart (1996), Atmospheric cosmic rays and energetic particles at aircraft altitudes, *Environ. Int.*, *22*, S9–S44.
- Parthasarathy, R. (1976), Mesopause dust as a sink for ionization, *J. Geophys. Res.*, *81*, 2392–2396.
- Ramanan, G., and G. R. Freeman (1990), Electron mobilities in low density helium and nitrogen gases: Momentum transfer cross sections at very low energies, *J. Chem. Phys.*, *93*(5), 3120–3125.
- Ramanan, G., and G. R. Freeman (1991), Electron mobilities in low density hydrogen and carbon monoxide gases: Momentum transfer cross sections at very low energies, *J. Chem. Phys.*, *95*(6), 4195–4200.
- Seiff, A., D. B. Kirk, T. C. D. Knight, R. E. Young, J. D. Mihalov, L. A. Young, F. S. Milos, G. Schubert, R. C. Blanchard, and D. Atkinson (1998), Thermal structure of Jupiter's atmosphere near the edge of the 5-mm hot spot in the north equatorial belt, *J. Geophys. Res.*, *103*, 22,857–22,889.
- Smith, D., and M. J. Church (1977), Ion-ion recombination rates in the Earth's atmosphere, *Planet. Space Sci.*, *25*, 433–439.
- Space Studies Board, National Research Council (2003), *New Frontiers in the Solar System: An Integrated Exploration Strategy*, Natl. Acad. Press, Washington, D. C.
- Tomasko, M. G., et al. (2005), Rain, wind and haze during Huygen probe's descent to Titan's surface, *Nature*, *438*(8), 765–778.
- Twomey, S. (1977), *Atmospheric Aerosols*, Elsevier, New York.
- West, R. A., K. H. Baines, A. J. Friedson, D. Banfield, B. Ragent, and F. W. Taylor (2004), Jovian clouds and haze, in *Jupiter: The Planet, Satellites and Magnetosphere*, edited by F. Bagenal, T. Dowling, and W. McKinnon, pp. 79–104, Cambridge Univ. Press, Cambridge, U. K.
- Wilson, A. (Ed.) (2004), *Proceedings of the International Workshop on Planetary Probe Atmospheric Entry and Descent Trajectory Analysis and Science*, Eur. Space Agency Spec. Publ., ESA-SP544.
-
- W. J. Borucki, NASA Ames Research Center, MS 244-30, Moffett Field, CA 94035, USA.
- K. O'Brien, Department of Physics and Astronomy, Northern Arizona University, Flagstaff, AZ 86011, USA.
- S. N. Tripathi, Indian Institute of Technology, Kanpur 208016, India.
- R. C. Whitten, SETI Institute, 515 N. Whisman Road, Mountain View, CA 94043, USA. (rwhitten@pacbell.net)